Supporting Information

Photo-Induced Exciton Dynamics and Broadband Light Harvesting in ZnO Nanorod-Templated Multilayered 2D MoS_2/MoO_3 Photoanodes for Solar Fuel Generation

Keshab Karmakar,[1] Dipanjan Maity,[1] Debashish Pal,[2] Kalyan Mandal,[1] Gobinda Gopal Khan[2,*]

[1]Department of Condensed Matter Physics and Material Sciences, S. N. Bose National Centre for Basic Sciences, Block JD, Sector-III, Salt Lake, Kolkata 700 106, India.

[2]Department of Material Science and Engineering, Tripura University (A Central University), Suryamaninagar, Agartala, Tripura 799 022, India.

* Corresponding author E-mail:gobinda.gk@gmail.com, gobindakhan@tripurauniv.in

Synthesis of MoS_2 and MoO_3 layers on ZnO NRs

Herein, MoS_2 has been formed by thermal degradation of ammonium tetrathiomolybdate in inert atomosphere. The key reaction is: [1,2]

$$2(NH_4)_2MoS_4 \rightarrow MoS_3 + MoS_2 + 4NH_3\uparrow + 2H_2S\uparrow + S\uparrow \text{ (endothermic, 160-270°C)}$$

$$MoS_3 \rightarrow MoS_2 + S\uparrow \text{ (endothermic, 270-370°C)}$$

Whenever the annealing is conducted in air medium the MoS_2 turns into MoO_3.

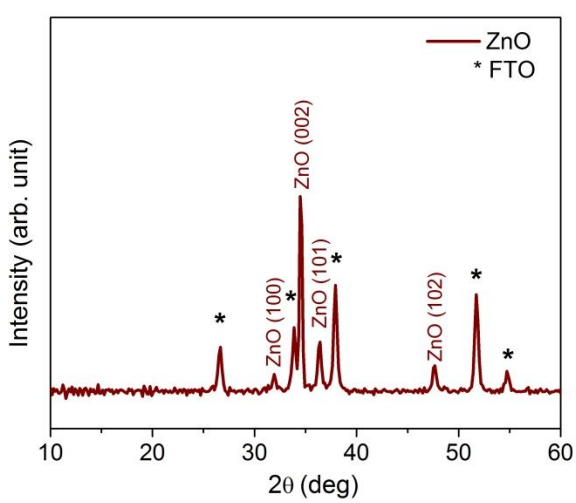

Fig. S1. GIXRD pattern of as fabricated pristine ZnO NRs arrays on FTO substrate.

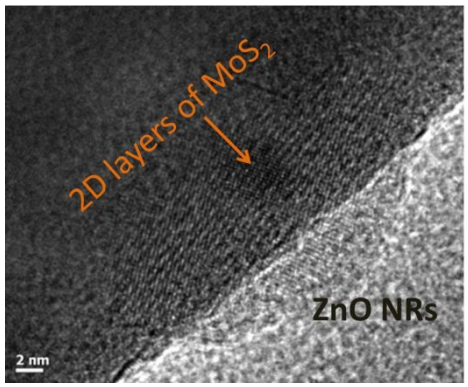

Fig. S2. High magnification TEM micrograph of ZnO/MoS_2 NHs.

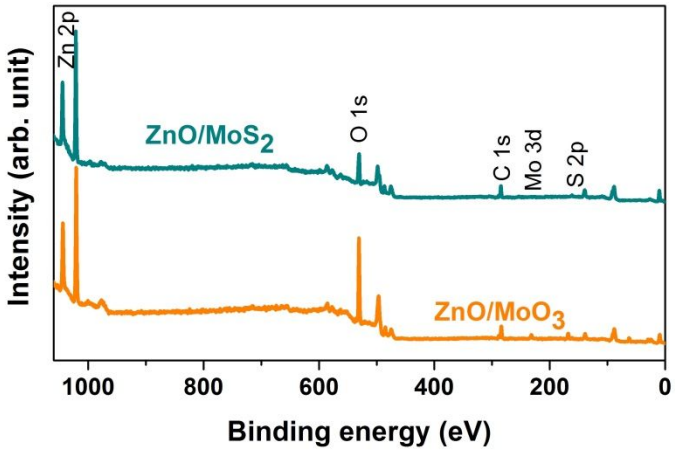

Fig. S3. XPS survey scan for ZnO/MoS_2 and ZnO/MoO_3 NHs.

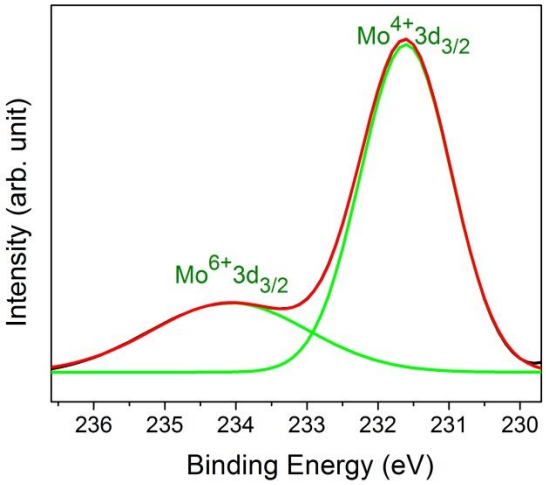

Fig. S4. Deconvulated XPS spectra of Mo 3d for ZnO/MoS_2 NHs.

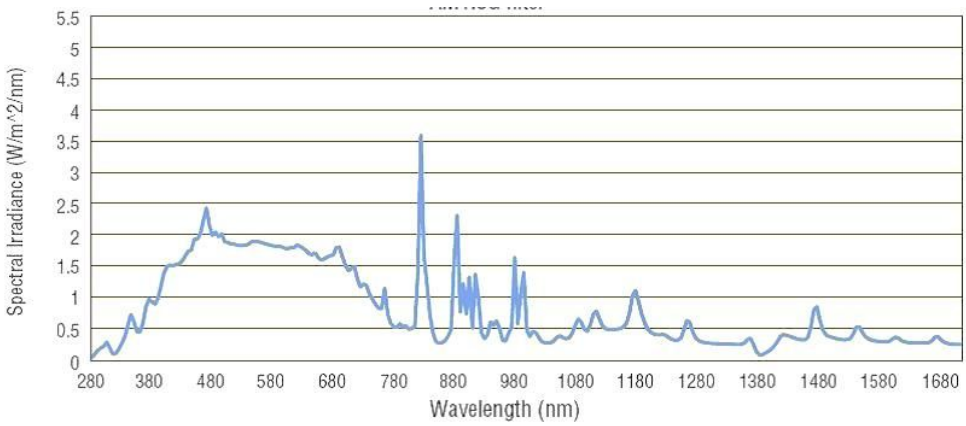

Fig. S5. Spectral output of the Solar Simulator with standard AM1.5G filter.

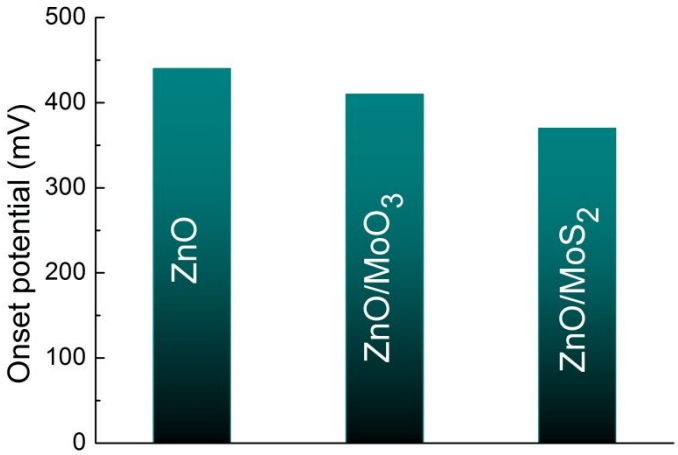

Fig. S6. Comparison of onset potential for the ZnO NRs, ZnO/MoO3 NHs and ZnO/MoS2 NHs.

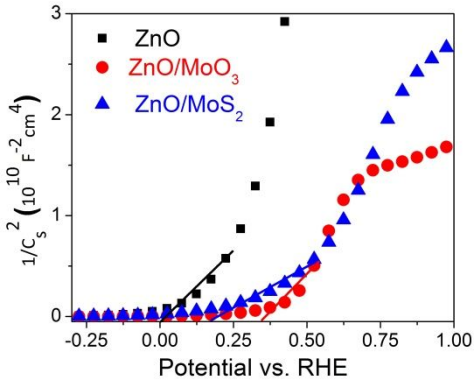

Fig. S7. Mott–Schottky plots of the photoelectrodes.

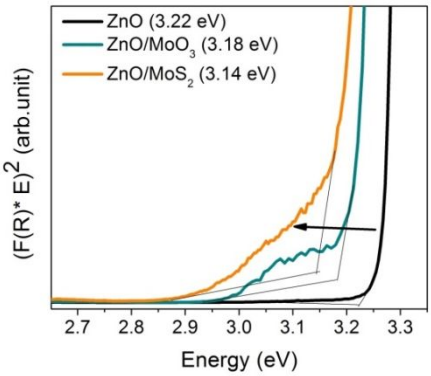

Fig. S8. Kubelka-Munk plots of the as prepared NHs.

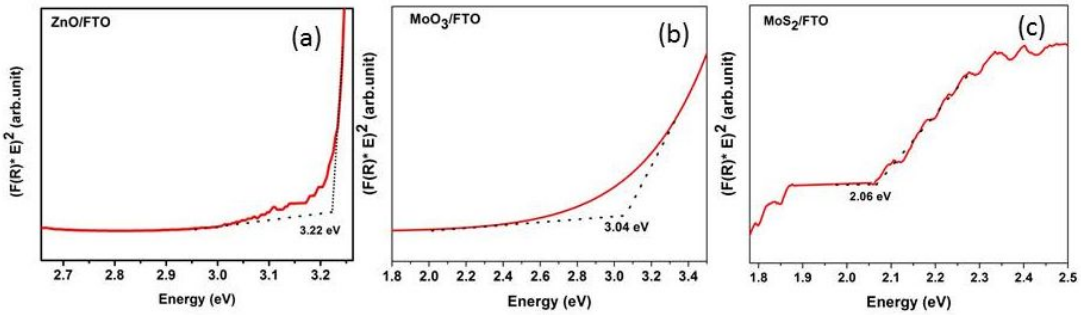

Fig. S9. Kubelka-Munk Plot of (a) ZnO NRs, (b) MoO_3 and (c) MoS_2 thin films grown on FTO.

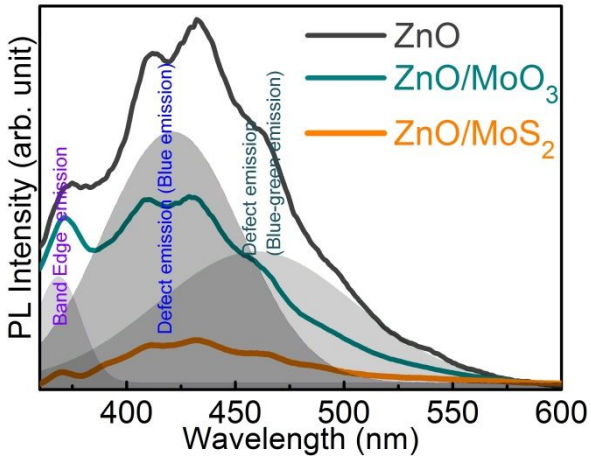

Fig. S10. Deconvoluted PL emission spectra of the ZnO NRs, ZnO/MoO3 NHs and ZnO/MoS2 NHs.

TRPL emission decay calculation

The TRPL decay curves were fitted by a bi-exponential decay model [3-6] with the decay kinetics function expressed as: $I(t) = \sum A_i\, e^{-t/\tau_i}$, where i = *1, 2*

The average PL emission lifetime, reflecting the overall emission decay behavior of the electrode samples, was calculated as[6]:

$$\tau_{avg} = \frac{\sum A_i\, \tau_i^2}{\sum A_i \tau_i}, \quad \text{where i} = 1, 2$$

Table S1. Electrochemical impedance parameters obtained from equivalent obtained from the EIS curves in Figure 5c.

Photoelectrodes	R_S (Ω)	R_{ct} (Ω)
ZnO NRs	14	2979
ZnO/MoO_3 NHs	16	1128
ZnO/MoS_2 NHs	9	506

Table S2: Summary of the photoelectrochemical performance of different ZnO-MoS_2 based photoelectrodes.

Sample Name/Photoelectrode	Incident radiation	ABPE Efficiency	Photocurrent density
MoS_2 flakes on ZnO [7]	100 mW/cm^2	--	1.7 mA/cm^2 at 0.5 V vs Hg/Hg_2Cl_2
MoS_2 nanosheet/ZnO nanowire [8]	AM1.5G, 100 mW/cm^2	--	0.6 mA/cm^2 at 1.2 V vs SCE
Few-layer MoS_2 flakes /ZnO[9]	AM1.5G, 100 mW/cm^2	0.9	1.4 mA/cm^2 at 0.4 V vs Hg/Hg_2Cl_2
ZnO-MoS_2-RGO Heterojunction[10]	Sunlight	--	5 mA/cm^2 at 1 V vs RHE
2D MoS_2/ ZnO NRs[Present work]	AM1.5G, 100 mW/cm^2	0.65	2 mA/cm^2 at 1.1 V vs RHE

References

1. Wang, H; Skeldon, P; Thompson, G; Wood, G. C. Synthesis and characterization of molybdenum disulphide formed from ammonium tetrathiomolybdate, *Journal of Materials Science* **1997** 32, 497-502.

2. Li, H; Ahn, S. H; Sang; Park, S; Cai, L; Zhao, J; He, J; Zhou, M; Park, J; Zheng, X. Molybdenum disulfide catalyzed tungsten oxide for on-chip acetone sensing, *Appl. Phys. Lett.* **2016**, 109, 133103.

3. Ning, Z.; Gong, X.; Comin, R.; Walters, G.; Fan, F.; Voznyy, O.; Yassitepe, E.; Buin, A.; Hoogland, S.; Sargent, E.H. Quantum-dot-in-perovskite solids. *Nature* **2015,** *523*, 324–328.

4. Wolf, C.; Lee, C.-L.; Im, S.H.; Heo, J.H.; Jeong, S.-H.; Myoung, N.; Sadhanala, A.; Park, M.-H.; Yoo, S.; Lee, T.-W.; Friend, R.H.; Kim, Y.-H.; Cho, H. Overcoming the electroluminescence efficiency limitations of perovskite light-emitting diodes. *Science* **2015,** *350,* 1222–1225.

5. Yang, M.Q.; Xu, Y.J.; Lu, W.; Zeng, K.; Zhu, H.; Xu, Q.H.; Ho, G.W. Self-surface charge exfoliation and electrostatically coordinated 2D hetero-layered hybrids. *Nat. Commun.* **2017**, *8*, 1–9.

6. Wu, H.; Kang, Z.; Zhang, Z.; Zhang, Z.; Si, H.; Liao, Q.; Zhang, S.; Wu, J.; Zhang, X.; Zhang, Y. Interfacial Charge Behavior Modulation in Perovskite Quantum Dot-Monolayer MoS_2 0D-2D Mixed-Dimensional van der Waals Heterostructures. *Adv. Funct. Mater.* **2018**, *28*, 1–10.

7. Trung, T.N.; Seo, D.-B.; Quang, N. D.; Kim, D.; Kim, E.-T. Enhanced photoelectrochemical activity in the heterostructure of vertically aligned few-layer MoS_2 flakes on ZnO. *Electrochimica Acta* **2018**, *260*, 150-156.

8. Li, H.; Dong, W.; Zhang, J.; Xi, J.; Du, G.; Ji, Z. MoS_2 nanosheet/ZnO nanowire hybrid nanostructures for photoelectrochemical water splitting, *J. Am. Ceram. Soc.* **2018,** *101* 3989–96.

9. Nguyen, T. D.; Man, T. M.; Nguyen, M. H.; Seo, D.-B.; Kim, E-T. Effect of few-layer MoS_2 flakes deposited ZnO/FTO nanorods on photoelectrochemical characteristic, *Mater. Res. Express* **2019**, 6, 085070.

10. Kumar, S.; Reddy, N. L.; Kushwaha, H. S.; Kumar, A.; Shankar, M. V.; Bhattacharyya, K.; Halder, A.; Krishnan, V. Efficient Electron Transfer across a ZnO–MoS_2–Reduced Graphene Oxide Heterojunction for Enhanced Sunlight-Driven Photocatalytic Hydrogen Evolution. *ChemSusChem* **2017**, *10*, 3588–3603.